Journal of Nanobiotechnology

RESEARCH

Open Access

# GelMA hydrogels reinforced by PCL@GelMA nanofibers and bioactive glass induce bone regeneration in critical size cranial defects

Chenghao Yu[1,2,4], Jinli Chen[4], Tianrui Wang[5], Yawen Wang[1,6], Xiaopei Zhang[1,6], Zhuoli Zhang[7], Yuanfei Wang[3*], Tengbo Yu[2*] and Tong Wu[1,6*]

## Abstract

**Background** The process of bone healing is complex and involves the participation of osteogenic stem cells, extracellular matrix, and angiogenesis. The advancement of bone regeneration materials provides a promising opportunity to tackle bone defects. This study introduces a composite hydrogel that can be injected and cured using UV light.

**Results** Hydrogels comprise bioactive glass (BG) and PCL@GelMA coaxial nanofibers. The addition of BG and PCL@GelMA coaxial nanofibers improves the hydrogel's mechanical capabilities (353.22 ± 36.13 kPa) and stability while decreasing its swelling (258.78 ± 17.56%) and hydration (72.07 ± 1.44%) characteristics. This hydrogel composite demonstrates exceptional biocompatibility and angiogenesis, enhances osteogenic development in bone marrow mesenchymal stem cells (BMSCs), and dramatically increases the expression of critical osteogenic markers such as ALP, RUNX2, and OPN. The composite hydrogel significantly improves bone regeneration (25.08 ± 1.08%) in non-healing calvaria defects and promotes the increased expression of both osteogenic marker (OPN) and angiogenic marker (CD31) in vivo. The expression of OPN and CD31 in the composite hydrogel was up to 5 and 1.87 times higher than that of the control group at 12 weeks.

**Conclusion** We successfully prepared a novel injectable composite hydrogel, and the design of the composite hydrogels shows significant potential for enhancing biocompatibility, angiogenesis, and improving osteogenic and angiogenic marker expression, and has a beneficial effect on producing an optimal microenvironment that promotes bone repair.

**Keywords** GelMA, Nanofiber, Bioactive glass, Organic-inorganic composite, Bone regeneration

*Correspondence:
Yuanfei Wang
zhizunbao19@163.com
Tengbo Yu
ytb8912@hotmail.com
Tong Wu
twu@qdu.edu.cn
[1]Medical Research Center, The Affiliated Hospital of Qingdao University, Qingdao University, Qingdao 266000, China
[2]Department of Orthopedic Surgery, Qingdao Municipal Hospital, University of Health and Rehabilitation Sciences, Qingdao 266071, China
[3]Central Laboratory, Qingdao Stomatological Hospital Affiliated to Qingdao University, Qingdao 266001, China
[4]Department of Sports Medicine, The Affiliated Hospital of Qingdao University, Qingdao University, Qingdao 266000, China
[5]Department of Traumatology, The Affiliated Hospital of Qingdao University, Qingdao University, Qingdao 266000, China
[6]Shandong Key Laboratory of Medical and Health Textile Materials, College of Textile & Clothing, Qingdao University, Qingdao 266071, China
[7]Radiology, Pathology, and BME, University of California Irvine, Irvine 92617, USA

© The Author(s) 2024. **Open Access** This article is licensed under a Creative Commons Attribution-NonCommercial-NoDerivatives 4.0 International License, which permits any non-commercial use, sharing, distribution and reproduction in any medium or format, as long as you give appropriate credit to the original author(s) and the source, provide a link to the Creative Commons licence, and indicate if you modified the licensed material. You do not have permission under this licence to share adapted material derived from this article or parts of it. The images or other third party material in this article are included in the article's Creative Commons licence, unless indicated otherwise in a credit line to the material. If material is not included in the article's Creative Commons licence and your intended use is not permitted by statutory regulation or exceeds the permitted use, you will need to obtain permission directly from the copyright holder. To view a copy of this licence, visit http://creativecommons.org/licenses/by-nc-nd/4.0/.

## Background

Dealing with bone tissue defects is a difficult task in the field of orthopedics, as a variety of factors, such as trauma, infections, tumors, osteonecrosis, and congenital malformations, can lead to bone tissue defects [1]. The conventional methods used to address these deficiencies, namely autografts, allografts, and xenografts, have well-established but restrictive characteristics, including restricted tissue supply and the possibility of rejection [2]. As a reaction, bone tissue engineering has developed as a promising approach to overcome these problems by developing composite biomaterials that improve bone regeneration. This encompasses the investigation of hydrogels, nanofiber membranes, and stem cells, all of which play a role in imitating bone's intricate organic and inorganic structural elements [3–5]. The organic matrix of bone is mainly formed of collagen fibers and polysaccharides. It is distinct from the inorganic phase, which comprises approximately 70% of the bone's composition and comprises hydroxyapatite and other minerals like magnesium and zinc [2, 6].

Bioactive glass (BG) is a biomaterial that has received significant study focus in bone repair due to its excellent biocompatibility, osteoconductive characteristics, and capacity to stimulate bone formation [7]. Hench identified 45S5 BG, which consists of 45% $SiO_2$, 24.5% CaO, 24.5% $Na_2O$, and 6% $P_2O_5$, as a graft material that enhances bone regeneration [8]. BG is exceptionally able to support bone growth, promoting a strong connection with surrounding bone tissue due to its highly active surface. It contains a large amount of ions, and upon contact with human fluids, amorphous calcium phosphate forms on the surface, eventually turning into hydroxyapatite crystals [9]. The complex interaction between dissolved ions and cellular entities influences the process of bone regeneration on BG [10]. These ions can enhance the growth and activity of osteoblasts, leading to increased cell division, higher levels of protein production, and improved mineralization [11]. Furthermore, these ions can potentially enhance the differentiation of bone marrow mesenchymal stem cells (BMSCs) into bone cells and the formation of blood vessels in damaged tissues [12, 13]. To improve the effectiveness of therapy, specific metallic ions such as strontium, zinc, silver cerium, and gallium are added to the composite materials to enhance the regenerative effect [14–16].

Hydrogels are three-dimensional (3D) network scaffolds made of biocompatible cross-linked hydrophilic polymers that can be used for tissue engineering repair. Hydrogels provide a growth environment similar to the natural extracellular matrix (ECM), allowing for the transport and regulated release of growth factors, cells, and a variety of bioactive components, which are essential for bone tissue repair. Gelatin contains various ECM components and has good biocompatibility and biodegradability [17]. Gelatin and side chain modified products are utilized to make hydrogels. The photoinitiators, ultraviolet (UV), and visible light can crosslink and cure gelatin methacrylate (GelMA), a double-bonded gelatin derivative. GelMA combines natural and synthetic biomaterials with highly thermosensitive gel qualities and degradability, good biocompatibility and cellular activity, and a 3D geometry that promotes cell development and differentiation. Thus, it can replace synthetic basement membranes and other collagen hydrogels [18]. Through injection, complete filling, and light-facilitated covalent crosslinking, GelMA could distribute gel to uneven defect areas [19]. Nanofiber-reinforced composites have better mechanical characteristics than hydrogels [20]. Polycaprolactone (PCL)@GelMA nanofiber-reinforced composite hydrogels with core-shell structure can be prepared by improved coaxial electrospinning technique, thus improving their mechanical properties.

This study created photo-crosslinked GelMA/BG nanofiber composite hydrogels by combining coaxial fibers and BG with the GelMA hydrogel. The composite hydrogel has exceptional biocompatibility, mechanical characteristics, and the potential to induce osteogenic differentiation. The experiment examined the influence of different BG content and the presence or absence of coaxial fibers on the hydrogel's overall physical and chemical characteristics. Additionally, in vitro research was performed to evaluate cells' vitality and differentiation, while in vivo investigations investigated their impact on bone repair after creating a lesion (Scheme 1).

## Materials and methods

### Materials

Type A gelatin, PCL, and Triton X-100 were purchased from Sigma (Germany). BG was bought from Hannotech Biosciences (China). The photoinitiator (lithium phenyl-2,4,6-trimethylbenzoylphosphinate, LAP) and portable curing light source (405 nm, 3 W) were bought from EngineeringForLife (China). Hexafluoroisopropanol (HFIP) and methacrylic anhydride (MA) were obtained from Macklin (China). Matrigel matrix was bought from Becton, Dickinson and Company (USA). Electrospinning machines were purchased from Yongkang (China). Fetal bovine serum (FBS) was obtained from Gibco (USA). Phosphate-buffered saline (PBS), Dulbecco'smodified Eagle medium (DMEM), penicillin-streptomycin solution (PS), ethylene diamine tetraacetic acid (EDTA) solution, cell counting kit-8 (CCK-8), SP Kit (Rabbit), hematoxylin-eosin staining (H&E), Masson's trichome staining, Calcein-AM/Propidium iodide (Calcein-AM/PI) kit and Radioimmunoprecipitation assay lysis buffer (RIPA lysates) were purchased from Solarbio (China). CD45, CD29, and Rabbit Anti-Osteopontin antibodies were

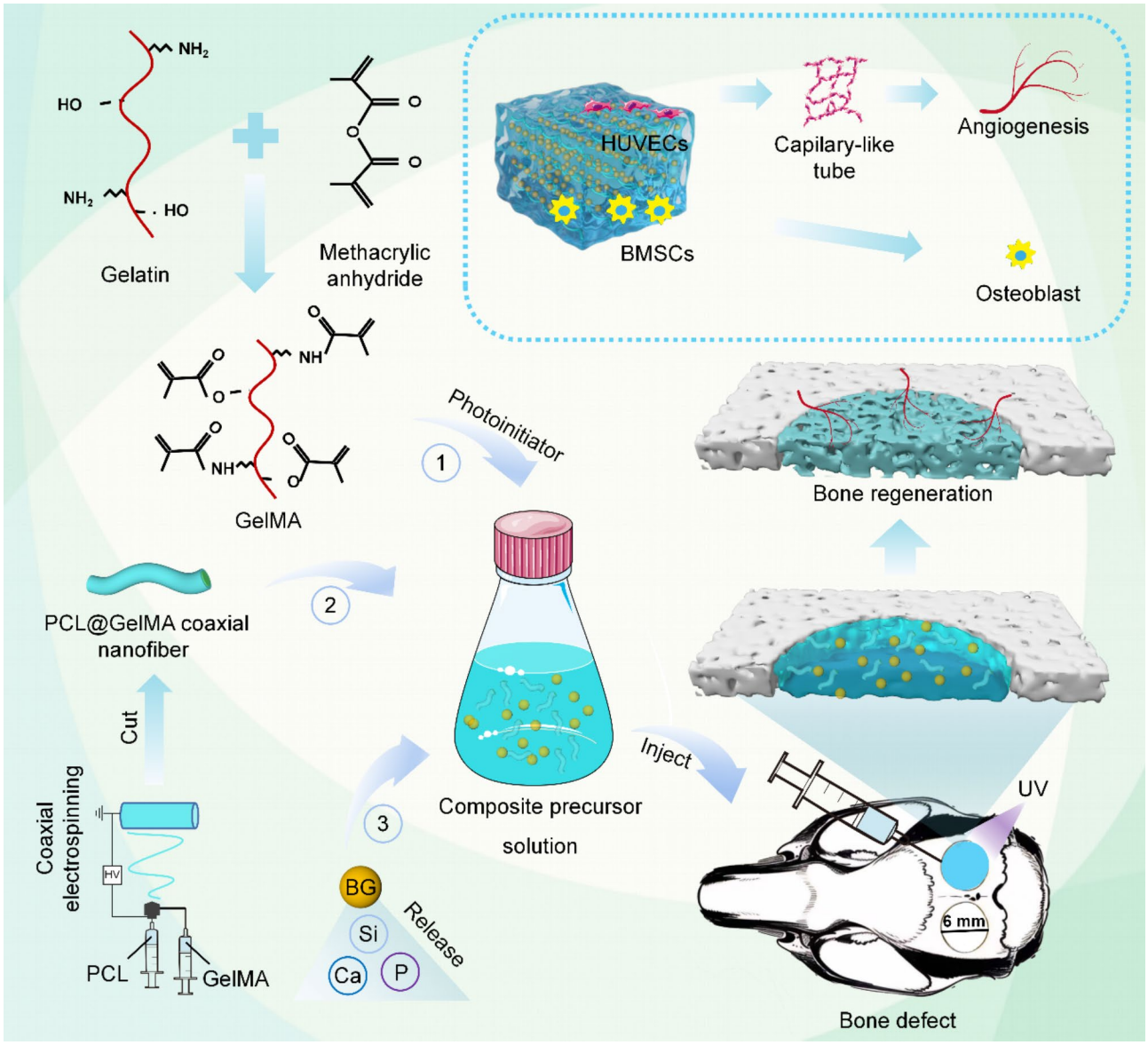


**Scheme 1** Schematic illustration of the fabrication process, the excellent angiogenic and osteogenic properties, and the corresponding underlying mechanism of the composited hydrogel scaffold

purchased from Bioss Biotechnology Co., Ltd. (China). FITC Anti-Rat CD 45 antibody and PE Anti-Rat CD 29 antibody were purchased from Elabscience (China). Anti-CD31 antibody and Phalloidin-iFluor 488 antibody were purchased from Abcam (UK). FastPure Cell/Tissue Total RNA Isolation Kit V2, ChamQ Universal SYBR qPCR Master Mix, and HiScript III RT SuperMix for qPCR were bought from Vazyme (China). Gene primers of Actin, alkaline phosphatase (ALP), runt-related transcription factor 2 (RUNX2), and osteopontin (OPN) were purchased from Sangon Biotech (China). All reagents were taken for direct use without further treatment.

## Methods

### *Preparation and characterization of GelMA hydrogel*

Briefly, 2 g of type A gelatin was added to 20 mL of PBS at 60 °C and dissolved. Subsequently, 1.6 mL of MA was dropwise added into the solution at a rate of 1.0 mL/h while stirring vigorously for 3 h, followed by adding 80 mL of preheated PBS. The unreacted components were removed in deionized water using a 12–14 kDa dialysis tube for one week. Subsequently, the fluid was filtered through a 0.22 μm filter, and the resulting liquid was frozen at -80 °C overnight and then lyophilized. The GelMA solution was prepared by dissolving the lyophilized GelMA (0.7 g) in 10 mL of PBS containing photoinitiator (0.5% w/v) at 60 °C. Subsequently, the GelMA solution

was freeze-dried, coated with Au/Pd using a Hummer 6 sputter (Anatech, Union City, CA), and imaged utilizing a Phenom Pure scanning electron microscope (SEM, Shanghai, China), and the success of the GelMA fabrication was tested using Nuclear Magnetic Resonance Spectra (NMR, Bruker Avance DPX Company).

#### *Fabrication of PCL@GelMA coaxial nanofibers*

The electrospinning equipment was utilized to fabricate a core-shell structure, where PCL (10 wt%) served as the core and GelMA (10 wt%) acted as the shell, dissolved in HFIP. A high voltage of 15 kV was applied between the collector and the coaxial needle, which was separated by a distance of 15 cm. The two solutions were injected using two independent syringe pumps at 1 mL/h (shell) and 0.5 mL/h (core). The coaxial needle used an inner diameter of 0.34 mm and an outer diameter of 0.84 mm. After 2 h, the electrospinning process was terminated. Subsequently, the collected coaxial fiber membranes were immersed in absolute ethanol containing 1% photoinitiator and subjected to UV irradiation for 1 h to obtain the solid GelMA. The coaxial fiber membrane was coated with Au/Pd using a Hummer 6 sputter and then imaged using SEM. Transmission electron microscope (TEM) imaging was performed to validate the presence of coaxial fibers. The average diameter of the nanofibers was measured using ImageJ software from 100 nanofibers in the SEM images. The success of the coaxial fibers and their integrity after treatment with ethanol were verified using an Fourier Transform Infrared Spectroscopy (FT-IR) spectrometer. To enhance dispersion and ensure injectability following hydrogel addition, the coaxial fibers were sectioned into shorter lengths utilizing a freezing microtome (Leica, Germany).

#### *Fabrication and characterization of GelMA-PCL@GelMA-BG composited hydrogel*

The GelMA-PCL@GelMA-BG composite hydrogels were prepared by incorporating coaxial short PCL fibers (2% w/v) and varying masses of BG (0, 1, 5, 10, 20% w/v) into the GelMA solution. Upon exposure to UV light for 10 s, the hydrogels transitioned from liquid phase to solid state. A rheometer was used to ascertain the alteration in modulus of the diverse composite hydrogels throughout the transformation from liquid to gel state. The hydrogels were subjected to freeze-drying after fabrication to examine their surface morphology. The composite hydrogels were coated with Au/Pd using a Hummer 6 sputter and then imaged using SEM. The composite hydrogels were assessed for swelling, hydration, degradation, mechanical properties, and ability to form apatite. The prepared composite hydrogels ($n=5$) were first equilibrated in PBS at 37 °C for 24 h. The weights of the samples before hydration ($W_o$) and at different time points ($W_t$) were recorded, respectively. The swelling ratio of the samples was calculated according to the following equation:

$$\text{Swelling ratio } (\%) = \frac{W_t - W_o}{W_o} * 100$$

The hydration degree of samples was calculated according to the following equation:

$$\text{Hydration degree } (\%) = \frac{W_t - W_o}{W_o} * 100$$

The mechanical properties of the composite hydrogels were evaluated using a mechanical testing machine (Instron, USA). Cylindrical samples ($n=3$) of 10 mm diameter and 4 mm thickness were immersed in PBS for 24 h before testing. The uniaxial compression experiment was conducted at a 1 mm/min strain rate, and the stress-strain curve was used to calculate the peak stress and compression modulus.

The degradation properties of the composite hydrogels were assessed by subjecting them to simulated body fluid (SBF) or collagenase (Sigma, USA), which mimicked in vivo conditions. The initial weight of the lyophilized samples ($n=5$) was recorded as $W_i$. Subsequently, the samples were incubated on a shaker in SBF or PBS containing collagenase (2.5 U/mL) at 37 °C. The samples' final weight ($W_f$) was measured at different time points (0 h, 6 h, 12 h, 18 h, 24 h, 48 h, and 72 h, and on days 7, 14, and 28). The weight% of the remaining samples was calculated using the following equation:

$$\text{Mass remaining } (\%) = \frac{W_f}{W_i} * 100$$

To assess the apatite-forming capability of the composite hydrogels, triplicate samples ($n=3$) were immersed in SBF for 7 days. Subsequently, the collected samples were washed three times, lyophilized, and examined using SEM and energy-dispersive X-ray spectroscopy (EDS).

#### *Effect of composite hydrogels on cell proliferation*

The cell viabilities of the different composite hydrogels were evaluated using CCK-8. MC3T3-E1 cells were cultured in the immersed complete medium of various hydrogels for 1, 3, and 7 days, followed by a CCK-8 assay, and tissue culture plates were used as controls. At each time, cells were triple-washed with PBS and then incubated with the culture medium containing 10% CCK-8 reagent for 2 h. The supernatant absorbance at 450 nm was measured using a microplate reader. Calcein-AM/PI (live/dead) staining was performed on day 3, and images were captured using an inverted microscope (Olympus, Japan) and analyzed with ImageJ software.

#### *Cell adhesion on composed hydrogels in vitro*

After sterilization, the composite hydrogels were mixed in a sterile laminar flow hood and solidified under UV light in a 24-well plate to assess cell adhesion. MC3T3-E1 cells were seeded onto the hydrogel surface at a density of $2\times10^4$ cells/well and cultured with complete medium (DMEM supplemented with 10% FBS, 1% penicillin/streptomycin) at 37 °C in a 5% $CO_2$ environment. After 3 days of culture, the cell-seeded hydrogels were fixed with 3% glutaraldehyde (Sigma, USA) for 30 min and washed three times with deionized water. Subsequently, the hydrogels containing cells were lyophilized and examined using SEM.

#### *Angiogenesis of composed hydrogels in vitro*

The tube formation and scratch assays were conducted using HUVECs. The preparation of extracts entailed the soaking of various composite hydrogels in DMEM for 72 h, in accordance with the guidelines in ISO 10993-12. Subsequently, the HUVECs were treated with the diluted extract for 24 h. A mixture of 50 μL of Matrigel matrix and DMEM at a 1:1 ratio was added to a 24-well plate and incubated at 37 °C for 30 min to form a gel state. Subsequently, the HUVECs were seeded onto Matrigel at a density of $5\times10^4$ cells/well for 6 h. Thereafter, the tube structures formed within the gel were imaged using a microscope, and the parameters associated with tube formation were measured using the ImageJ software. To investigate the influence of composite hydrogels on cell migration, longitudinal scratches were made when HUVECs reached approximately 90% confluence. The cells were cultured in the extraction DMEM solution of the composite hydrogels at 37 °C for 24 and 48 h, respectively. Then, the cells were stained with Calcein-AM and observed by the fluorescence microscope and photographed. The relative migration rate was measured using ImageJ software.

#### *Effect of composite hydrogels on cell osteogenic differentiation in vitro*

ALP activity was utilized to assess the impact of composite hydrogels on the differentiation of BMSCs. BMSCs were seeded in a 24-well plate at a density of $2\times10^4$ cells/well. After 24 h, the culture medium was replaced with the osteogenic supplemental medium derived from various composite hydrogels and maintained for 7 and 14 days. After rinsing three times with PBS, the cells were fixed with 4% paraformaldehyde, stained with alizarin red for 30 min, and washed thrice again with PBS. Images were acquired using an inverted microscope and analyzed utilizing ImageJ software. For quantitative analysis of ALP content, an ALP activity assay kit was employed to detect active components of ALP, and the absorbance of the supernatant was measured at 405 nm. To further evaluate the effect of composite hydrogels on the osteogenesis of BMSCs, osteogenesis-related genes (ALP, RUNX2, and OPN) were investigated. The total RNA was extracted using the FastPure Cell/Tissue Total RNA isolation kit, and an equivalent amount of RNA was processed to generate cDNA using the HiScript III RT SuperMix for the qPCR kit. Quantitative PCR was performed with ChamQ Univeral SYBR qPCR Master Mix.

#### *Effect of composite hydrogels on osteogenesis in vivo*

Four experimental groups of GelMA containing 20% BG and/or short coaxial fibers, respectively, were used to investigate the in vivo calcification ability of the composite hydrogels. The rats were anesthetized by isoflurane inhalation with an animal anesthetic machine (1 L/min). Sterile lyophilized hydrogels were implanted subcutaneously in 8-week-old Sprague Dawley (SD) rats, and samples were collected at 2 and 4 weeks for Micro-computed Tomography (Micro-CT) examination to assess bone production. The animal experiments were conducted following the approved protocol by the Animal Ethics Committee of Qingdao University (No.20210901SD5020231101128). To further investigate the impact of composite hydrogels on bone regeneration, an in vivo study was conducted using a critical-sized cranial bone defect model created in 8-week-old male SD rats. A 6 mm diameter defect was surgically induced on the cranial bone, followed by implantation of sterilized GelMA/BG-Fiber, GelMA/BG, GelMA/Fiber, and GelMA scaffolds into the defect site. The SD rats were raised and allowed to move freely for 4, 8, and 12 weeks. SD rats were euthanized with chloral hydrate overdose at the corresponding time points, and their cranial bones were collected and fixed in 10% formalin for 24 h. After photography and Micro-CT, samples were decalcified with 10% EDTA solution for 8 weeks. Subsequently, the samples were embedded in paraffin and sectioned into slices of 4 μm thickness. These sections were then stained for H&E, Masson's trichrome stain, as well as immunohistochemical markers including OPN, RUNX2, and CD31.

#### Statistical analysis

The comparison between groups was conducted using one-way analysis of variance (ANOVA), followed by Student's t-tests for all pairwise comparisons. All values were obtained from at least three independent replicates and are presented as mean ± standard deviation. $^{*}p<0.05$, $^{**}p<0.01$, $^{***}p<0.001$.

## Results and discussion

#### Characterizations of GelMA/BG-Fiber composite hydrogels

As GelMA is a partially synthetic polymer derived from gelatin, the hydrolyzed form of type I collagen found in

bone, we anticipate that utilizing this polymer to synthesize nanocomposite biomaterials for bone repair and regeneration could yield significant advantages. The synthesis of GelMA offers several benefits, such as enabling control over reproducibility, degree of methacryloyl substitution, and consequently, the initial mechanical properties of GelMA hydrogel [21]. Firstly, we observed the injectable properties of the synthesized GelMA and the composite hydrogel, which can be passed through a syringe needle and fill irregular defects (Fig. S1a-b). The rheometer results demonstrated that a range of composite hydrogels transitioned from liquid to gel in UV light irradiation (Fig. S1c-d). The storage modulus (G') increased with incorporating BG (Fig. S1e). The successful synthesis of GelMA enabled observation of its porous structure using SEM imaging techniques (Fig. S2a). The average pore size of GelMA was 110±27 μm (Fig. S2b). The pore sizes of different groups of hydrogels were also measured, and found that as the BG component content increased, the pore size of the hydrogel became smaller. Besides, the pore sizes of the hydrogel can be maintained by adding the PCL@GelMA coaxial fibers (Fig. S2c). Maintaining pore size provides an environmental basis for cell ingrowth and nutrient exchange, which is benefite for bone regeneration. Confirmation of gelatin modification with MA was achieved through NMR analysis (Fig. S2d) [22]. A comparative examination of gelatin and GelMA revealed a distinct double-bonded proton peak (=$CH_2$) in the NMR spectrum of GelMA, which appeared at approximately 5.5 ppm. An additional minor peak at 5.85 ppm can be attributed to the acrylic protons originating from MA groups [23]. Meanwhile, the disappearance of the peak associated with lysine-$NH_2$ (2.8 ppm) indicated the predominant grafting of MA onto lysine-$NH_2$ groups within the gelatin backbone during the formation of GelMA [24]. Additionally, the new peaks at 5.4 and 5.6 ppm indicated the successful binding of the methacrylate groups to gelatin. The degree of methacrylation of GelMA was calculated to be ≈71.89±0.33% as determined by the ratio of the integrated area of the lysine methylene signals (2.8-3.0 ppm) of GelMA and the phenylalanine signal (7.1–7.4 ppm) of unmodified gelatin [25].

PCL@GelMA coaxial nanofibers were fabricated successfully and observed by SEM and TEM (Fig. S3a). The inner layer (PCL) and outer layer (GelMA) can be seen in the TEM images. By measuring the SEM image, the diameter of the coaxial fiber was 879±207 nm (Fig. S3b). The application of FT-IR revealed that the collagen peak (1645.12) remained after the ethanol production process, which contributed to the successful fabrication of coaxial fibers (Fig. S3c). Consequently, GelMA hydrogel was augmented with coaxial fibers to fabricate a fiber-reinforced hydrogel system. By employing GelMA as the outer layer of the coaxial fibers, it is anticipated that superior adhesion between the outer layer and the surrounding GelMA hydrogel will be achieved during the UV crosslinking process, which will increase the overall strength through the formation of an interpenetrating network.

The GelMA/BG-Fiber composite hydrogels, containing varying concentrations of BG (0, 1, 5, 10, 20% w/v), with or without PCL@GelMA coaxial nanofibers, were successfully synthesized and can be crosslinked using UV light. Figure 1 shows that the short coaxial nanofibers with varying concentrations of BG were successfully incorporated while preserving the porous structure of the hydrogel. The porous structure of hydrogels is essential for cell growth and angiogenesis [26]. The composite hydrogels exhibited robust swelling properties due to their highly interconnected porous structure. The swelling of hydrogels plays a pivotal role in the healing and regeneration of bone tissue as it facilitates the transportation of nutrients and the removal of waste products through diffusion [21]. The incorporation of BG significantly influences the swelling behavior of the hydrogels. The swelling characteristics of the hydrogels decreased with the increase in BG content, which may be attributed to the electrostatic interaction between the negatively charged silicon hydroxyl (–Si–OH) groups on the surface of BG and the positively charged amino (–$NH_2$) groups in GelMA [9], whereas the incorporation of coaxial fibers had no significant effect (Fig. 2a-b). The hydration rate of the composite hydrogel with 20% BG-Fiber was 72%, which was lower than that of GelMA (89%) (Fig. 2c). The results demonstrate that the composite hydrogels exhibit favorable swelling ratios, which indicate their potential for efficient nutrient diffusion when transplanted into the body for bone regeneration.

The mechanical properties of the hydrogel were significantly enhanced by incorporating PCL@GelMA coaxial nanofibers and BG. The GelMA shell of the coaxial fiber exhibited a remarkable affinity with the surrounding GelMA hydrogel, facilitating crosslinking under UV light irradiation and thereby augmenting the overall mechanical characteristics. During compression performance testing, the composite hydrogel containing PCL@GelMA coaxial nanofibers exhibited rupture at a compression level of 65%. Remarkably, upon completion of the test, the composite hydrogel fully recovered its initial appearance, whereas the absence of PCL@GelMA coaxial nanofibers in the hydrogel resulted in irreversible fragmentation (Fig. S4a). The 2% concentration of PCL@GelMA coaxial nanofibers of the composite hydrogel, solely supplemented with PCL@GelMA coaxial nanofibers, exhibited a significantly higher value compared to the content of 0% and 1%, while no significant difference was observed in comparison to the 3% content (Fig. S4b). This result was similar to that of Qiu [20], and therefore, 2% PCL@

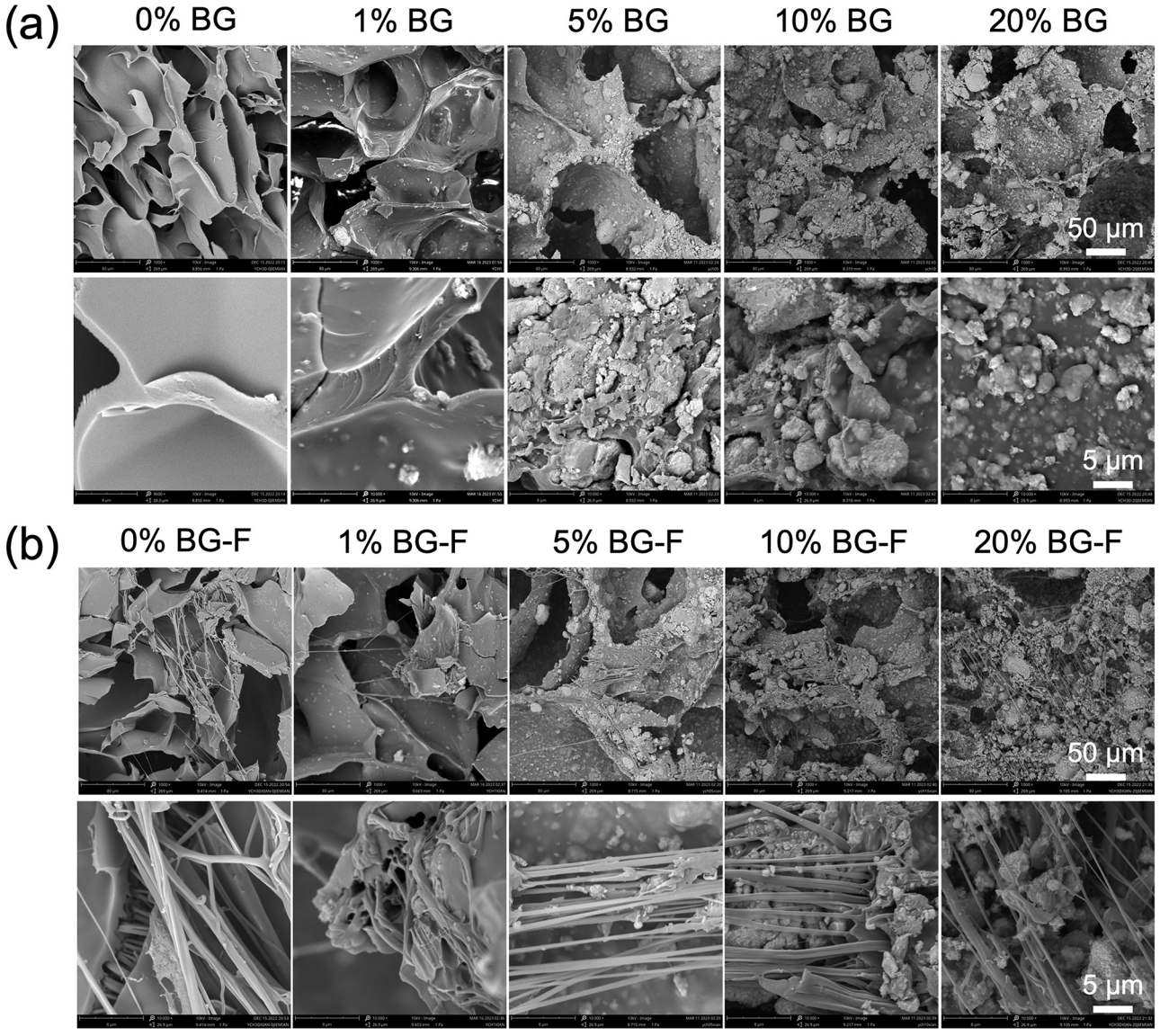


**Fig. 1** The SEM images of composite hydrogels. (**a**) Different BG contents (0, 1, 5, 10, 20% v/w) were added to GelMA. (**b**) Different contents (0, 1, 5, 10, 20% v/w) of BG and PCL@GelMA coaxial nanofibers added in GelMA

GelMA coaxial nanofibers were used in the subsequent experiments. The incorporation of PCL@GelMA coaxial nanofibers not only enhances the mechanical properties of the hydrogel but also maintains the hydrogel shape. The hydrogel exhibited a simultaneous increase in ultimate stress and compressive modulus with the addition of BG (Fig. 2d and Fig. S5a-b). The GelMA-containing BG hydrogels exhibited rupture at approximately 60% compression, whereas the composite hydrogel containing PCL@GelMA coaxial nanofibers exhibited rupture at a compression level of 65%. Notably, hydrogels with a BG content of 20% exhibited irrecoverable deformation when subjected to flat compression. Mechanical properties play a crucial role in the development of bone regeneration materials. Simple hydrogels possess limited mechanical strength and, therefore, necessitate the incorporation of PCL@GelMA coaxial nanofibers and BG to enhance the overall robustness. After incorporating these constituents, composite hydrogels retain their injectability and exhibit the potential for mending irregular bone defects.

The degradation properties of composite hydrogels are critical, and the optimal degradation scenario is the synchronization of hydrogel degradation and bone growth [27]. The degradation of composite hydrogels was assessed during a 28-day incubation period in SBF, approximating the duration required for bone healing and remodeling following fracture [21]. In SBF solution, the composite hydrogels containing 0%, 1%, and 5% BG exhibited significant degradation within two weeks and complete degradation by 4 weeks, while the hydrogels

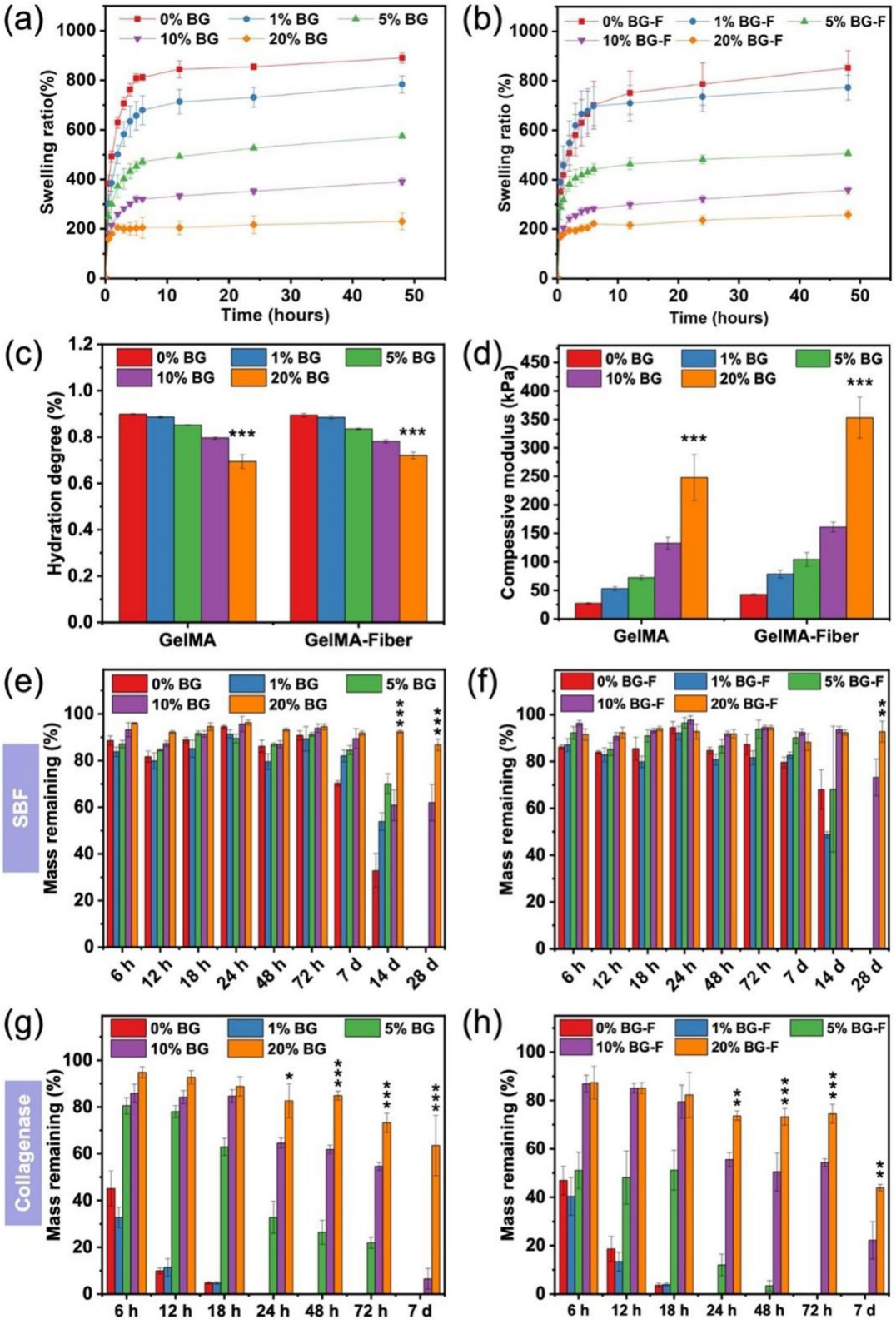


**Fig. 2** The effect of BG and coaxial fibers on composite hydrogels' hydration degree, mechanical, and physiological stability. (**a**-**c**) The swelling rate and hydration degree were weakened by adding BG and coaxial fibers. (**d**) The mechanical property was enhanced by adding BG and coaxial fibers. (**e**-**f**) Degradation behaviors of hydrogels in SBF showed slow weight loss after 28 days soaking. (**g**-**h**) Degradation behaviors of hydrogels in collagenase solution decreased the degradation rate by adding BG and coaxial fibers. (*$p < 0.05$, **$p < 0.01$, ***$p < 0.001$)

with 10% and 20% BG content demonstrated partial degradation (Fig. 2e-f). Collagenase-mediated degradation was rapid and complete within 24 h for hydrogels with 0%, 1%, and 5% BG content. Hydrogels containing 20% BG also exhibited significant degradation, reaching approximately 63% and 43% (fiber-containing) after 7 days (Fig. 2g-h). The addition of BG effectively slowed down the degradation process, possibly due to the strong interaction between BG and GelMA hindering the penetration of the collagenase solution. However, incorporating coaxial fibers did not significantly hinder the degradation, possibly due to the simultaneous degradation of the GelMA component in the shell and the hydrogel. The weight of the composite hydrogels exhibited fluctuations during the degradation measurements, which could be attributed to the hydrogel degradation along with the deposition of phosphates, which led to an increase in the weight of the sample. It can be inferred that the observed mass change is primarily attributed to the initial dissolution of the BG and the subsequent formation of mineralized crystals [28].

For the phosphate formation ability test, the composite hydrogels of each group were immersed in SBF for 7 days. Subsequently, the collected sample sections were examined using SEM. Particles were observed on the surface of the composite hydrogels, and EDS analysis revealed that these particles were enriched in calcium (Ca) and phosphorus (P) (Fig. S6a-b), which are the main components of bones. The composite hydrogel's Ca/P ratio of the surface elements was $1.56 \pm 0.03$, which resembles that in artificial bone (ranging from 1.50 to 1.67) [29]. The deposition of phosphate crystals on the surface gradually increases with increasing BG content (Fig. S6c), which could also be seen on the surface of the fibers (Fig. 3). In the presence of SBF, the composite hydrogels exhibited rapid release of calcium and phosphorus ions, forming calcium phosphate crystals on their surface [30]. Incorporating coaxial fibers also facilitates the nucleation and growth of phosphate crystals, enhancing their crystallization capacity [31]. In conclusion, incorporating BG and coaxial fibers significantly mitigated swelling and hydration rate, decelerated degradation kinetics, and augmented mechanical properties and mineralization formation ability of the composite hydrogels.

The inorganic components in bone biomaterials research include BG, β-tricalcium phosphate, and hydroxyapatite [32–34]. After implantation into damaged bones, BG is reabsorbed and integrated with the bone by forming a layer of apatite on its surface [35]. Although various polymers have been utilized in developing bone biomaterials, selecting polymers that closely emulate the natural bone microenvironment is imperative. Several studies have utilized both synthetic and natural polymers, such as chitosan, gelatin, and sodium alginate, to fabricate bone biomaterials containing BG [36–39]. The selection of gelatin, a natural polymer, is highly advantageous for establishing an environment that closely emulates the primary organic constituents of endogenous bones due to its hydrolyzed form derived from type I collagen present in the skeletal system. Collagen can enhance the metabolic activity of osteoblasts, thereby promoting osteogenesis, suppressing inflammation, inducing chondrogenesis, and improving bone mineral density [40]. Compared to gelatin, GelMA exhibited the primary advantage of a slower degradation rate and enhanced mechanical strength. In addition, the interaction between cells and the ECM is regulated by arginine-glycine-aspartic acid sequences within the GelMA structure, which serve as recognition sites for adhesive proteins that facilitate cell adhesion [41]. In summary, GelMA/BG-Fiber composite hydrogel is an excellent biomaterial that can effectively mimic the natural biological microenvironment of bone and has the potential to promote bone repair and regeneration.

#### Effect of composite hydrogels on cell behaviors in vitro

The interaction between cells and hydrogels is essential. Upon examination of the cells adhered to the surface of the composite hydrogels, it was observed that they exhibited strong adhesion, with even crystalline formations emerging on their surfaces during the sustained release of ions from the BG (Fig. 4a). This phenomenon became more pronounced with increasing BG content. We initially investigated the effect of fiber supplementation on cell proliferation and observed no statistically significant differences (Fig. 4d). The biocompatibility of different composite hydrogels was assessed using Calcein-AM/PI (live/dead) staining. It was observed that an increase in the content of BG resulted in a higher number of dead cells, and 83% of the cells survived in the 20% BG of composite hydrogel in the extraction solution (Fig. 4b-c). We attribute these results to crystal growth. The incorporation of BG has been shown to release a significant quantity of ions, resulting in an initial alkaline pH in the solution, which subsequently affects cell proliferation [42]. The growth and proliferation of stem cells are also influenced by the content of BG in solution, with cell growth being stimulated only at an appropriate concentration [43]. Therefore, in this experiment, we hypothesize that the development of crystals, changes in solution pH, and BG content in the solution exert an inhibitory effect on cell proliferation.

Angiogenesis and osteogenesis are essential for bone regeneration in tissue engineering scaffolds. The impact of hydrogels with varying BG contents on HUVEC tube formation assays was assessed. The composite hydrogel containing 20% BG exhibited the most extensive tube network formation, continuous

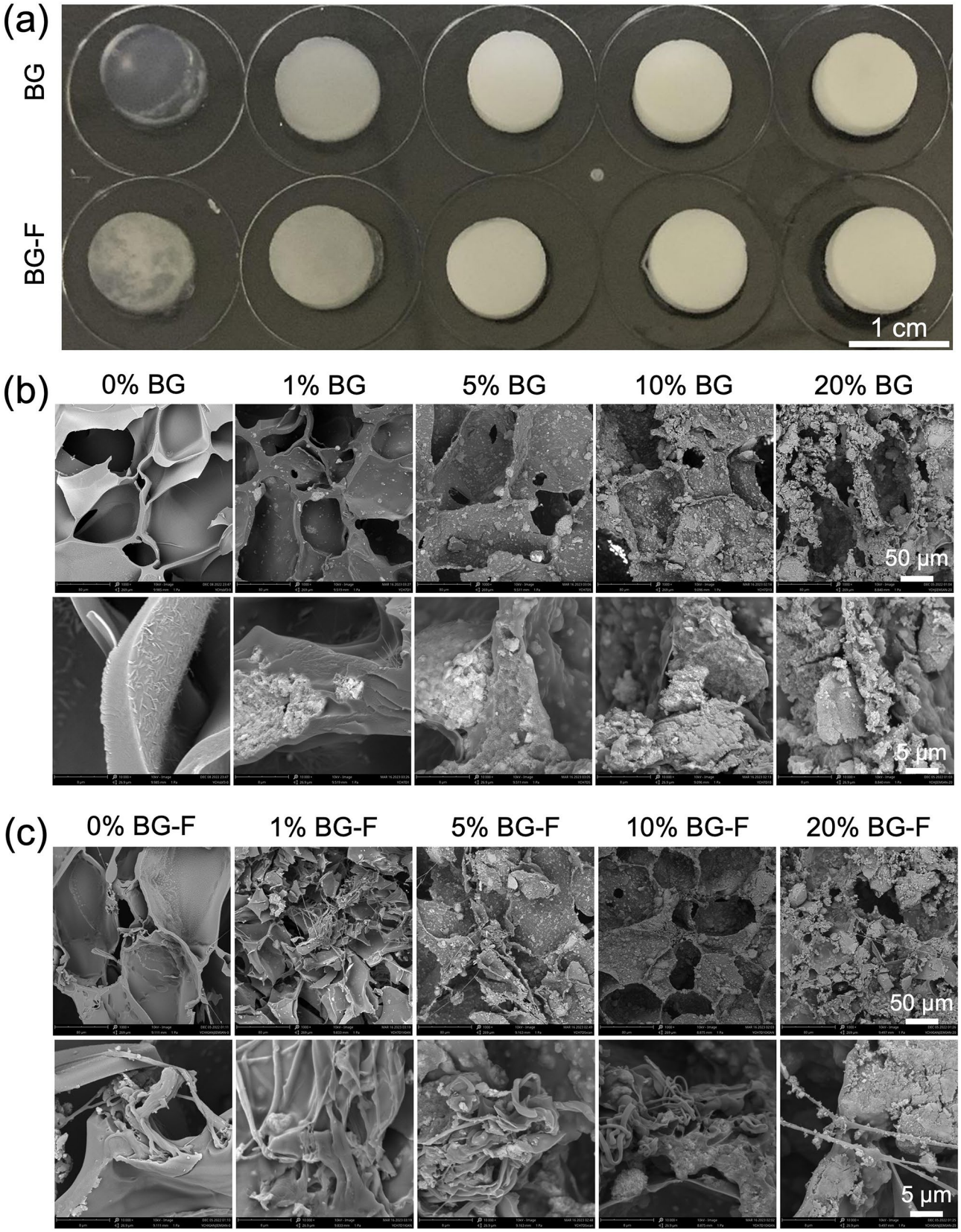


**Fig. 3** The optical pictures and SEM images of composite hydrogels soaked in SBF for 7 days. (**a**) The optical pictures of different groups. (**b**) The formation of mineralized crystals on the surface increased with increased BG content. (**c**) Mineralized crystals form on the surface of the fibers

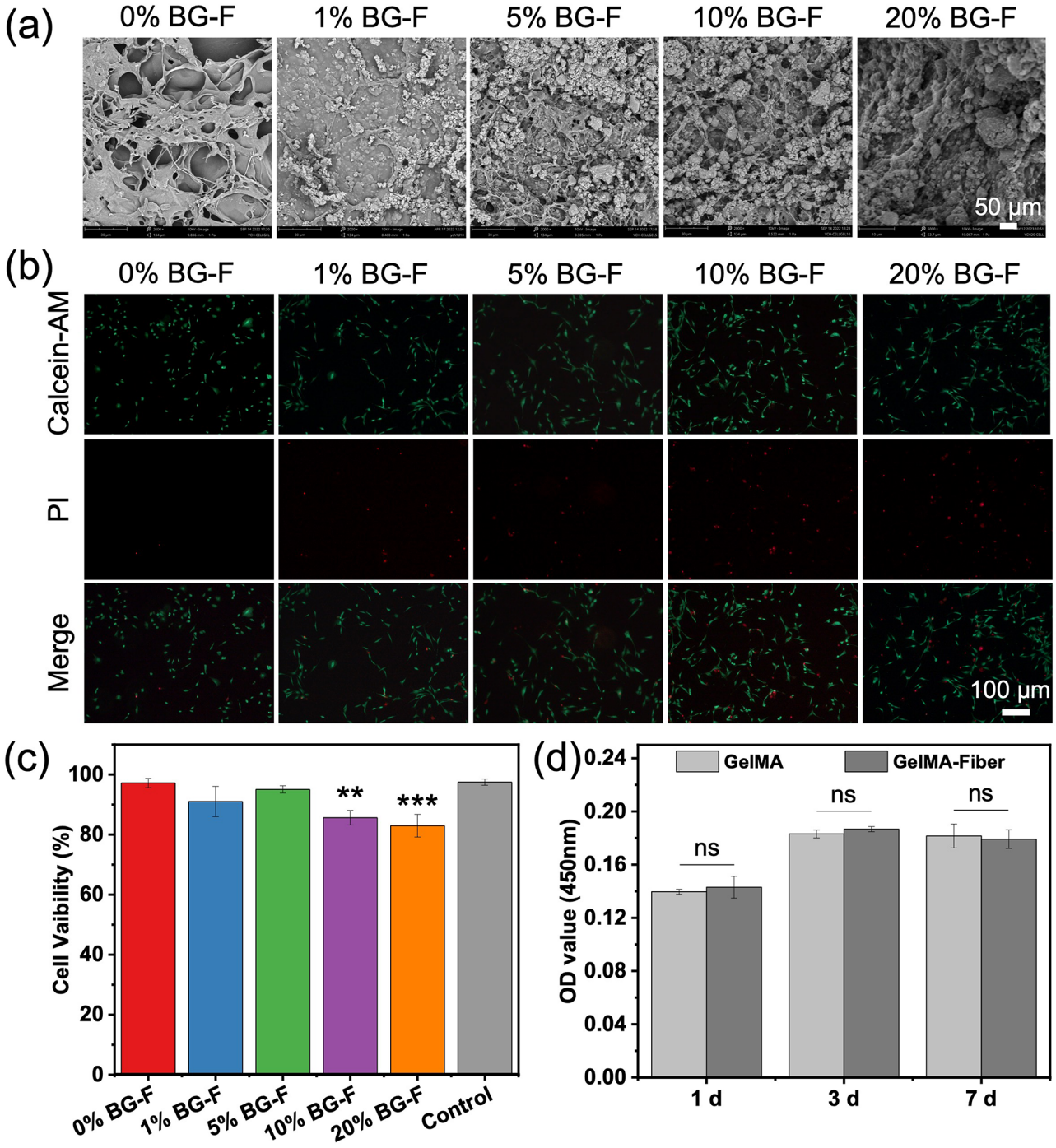


**Fig. 4** The evaluation of biocompatibility of composite hydrogels. (**a**) SEM images of MC3T3-E1 on composite hydrogels at day 3. (**b**) Calcein-AM/PI (live/dead) staining of different composite hydrogels. (**c**) Results of Calcein-AM/PI (live/dead) staining by counting the number of live cells. (**d**) The CCK8 assay showed that the cell growth was inhibited with the increase in BG. (*$p < 0.05$, ***$p < 0.001$)

tube walls, and the most significant number of meeting points, segments, and branches (Fig. 5a-d). Figure 5e shows cell migration images of HUVECs after culturing with the extraction solution of the composite hydrogels for 24 and 48 h. The corresponding quantitative migration areas filled by HUVECs are shown in Fig. 5f-g. The composite hydrogel containing 20% BG exhibited larger migration areas filled by HUVECs than the other groups. To assess the differentiating effect of hydrogels on cells, we isolated and characterized BMSCs based on their multipotent differentiation potential and cell surface-specific markers (Fig.

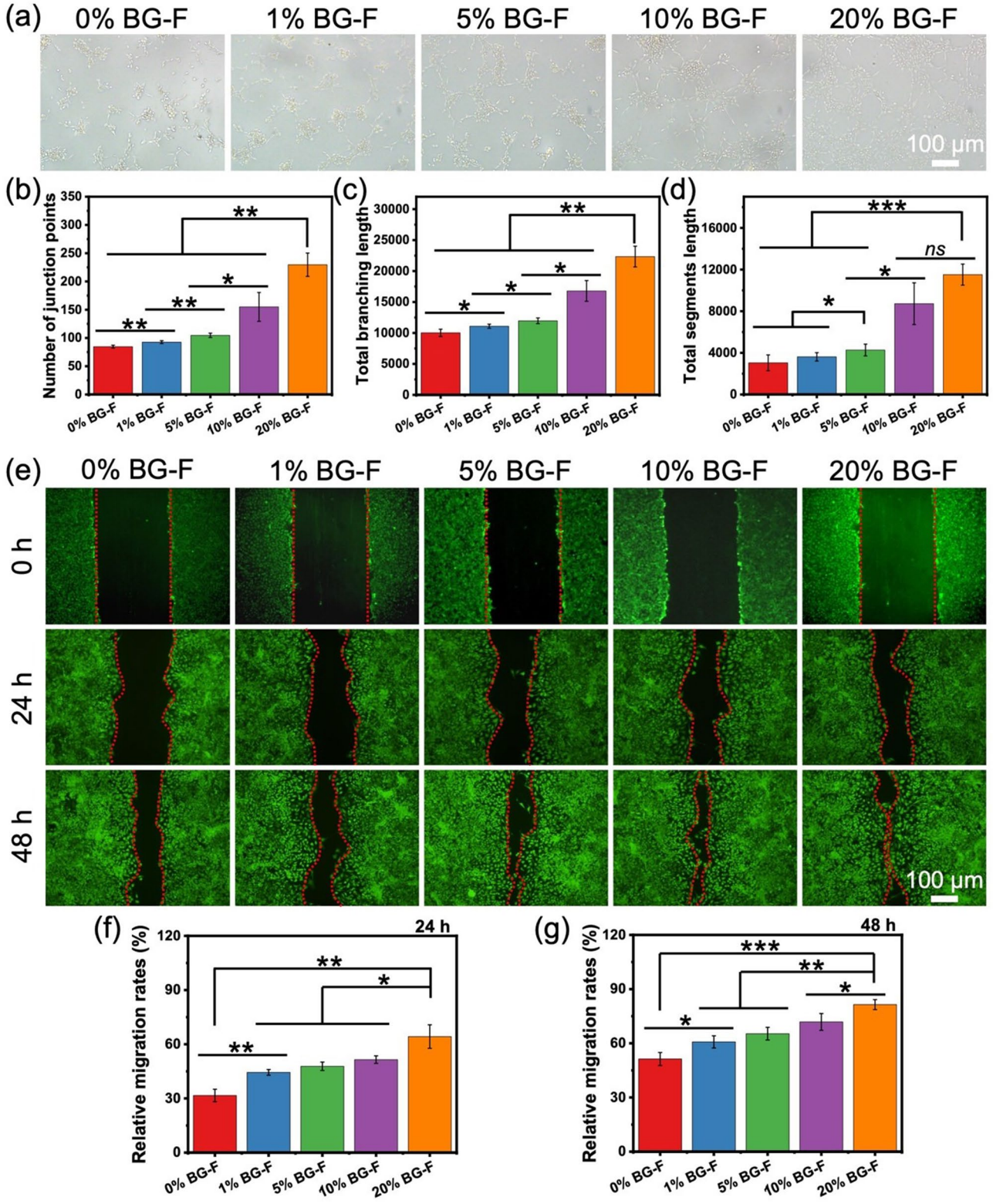


**Fig. 5** Effect of scaffolds on tube formation of angiogenesis. (**a**) Tube formation images of HUVECs. (**b**) Number of junctions, (**c**) total branching length, and (**d**) total segment length per field of view. (**e**) The images of HUVECs cultures for 24 and 48 h and (**f**, **g**) quantitative statistics of cell migration rates in cell scratch assay ($n = 3$). (*$p < 0.05$, **$p < 0.01$, ***$p < 0.001$)

S7) and then cultured BMSCs in the extraction solution of composite hydrogels. By evaluating the alizarin red staining of BMSCs cultured for 14 days, it was observed that the area of positive staining was significantly increased in the composite hydrogels containing 10% (9.7%) and 20% BG (12.8%) (Fig. 6a-b). Quantitative analysis of ALP showed that at 7 days, ALP expression was higher in the composite hydrogel containing 1% BG (0.24 U/L), while at 14 days, ALP expression was significantly increased in the composite hydrogel

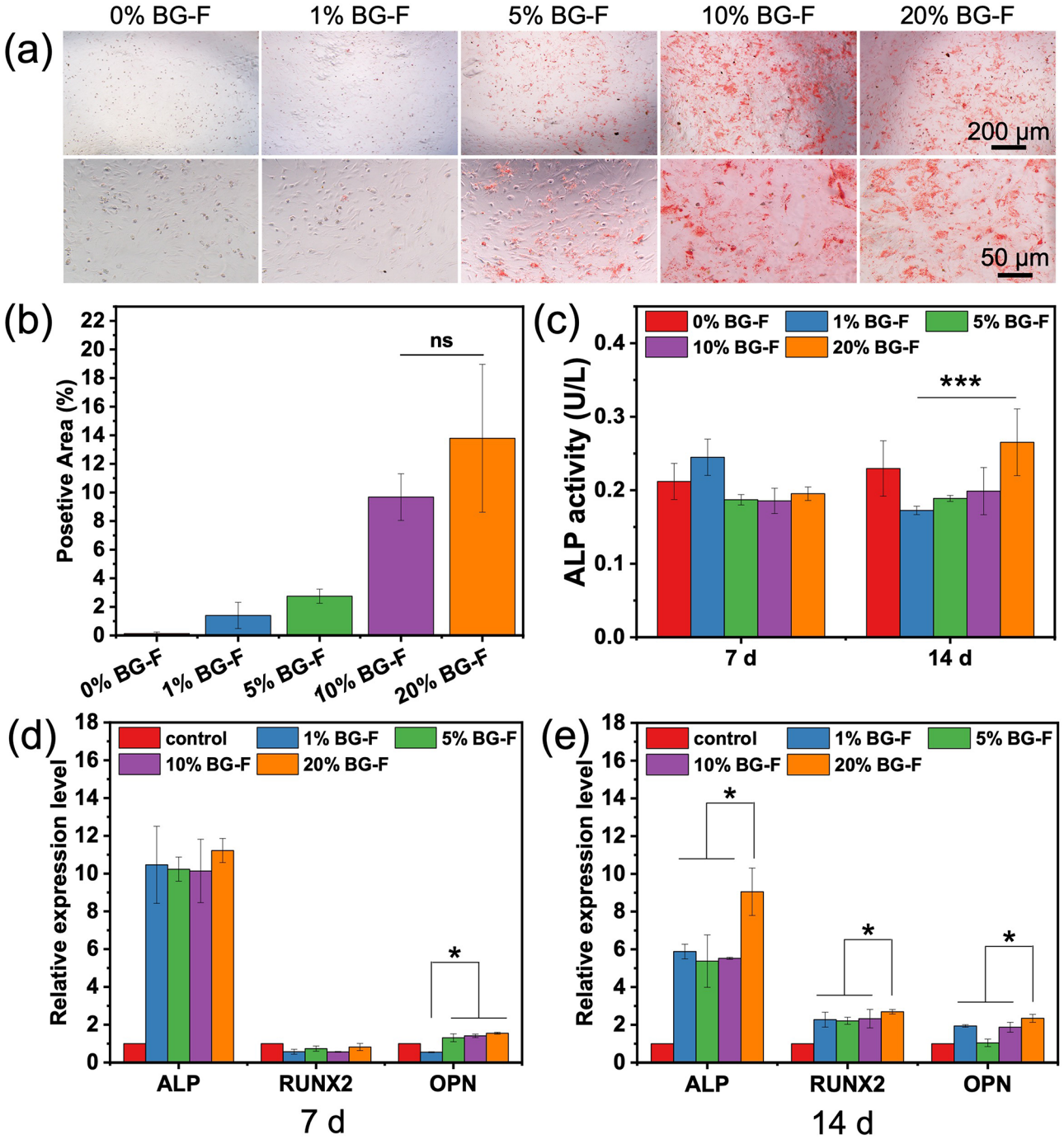


**Fig. 6** The osteogenic differentiation detected by alizarin red staining, ALP quantification, and qPCR. (**a**-**b**) Alizarin red staining after cultured BMSCs with the composite hydrogel extraction solution for 14 days. The 10% and 20% BG composite hydrogels can significantly increase the positive staining area. (**c**) Quantitative analysis of ALP shows that the expression of ALP in the composite hydrogel with 1% BG content was higher at 7 days, while the composite hydrogel with 20% BG content significantly promoted ALP expression at 14 days. (**d**-**e**) qPCR results detecting the osteogenic gene (ALP, RUNX2, and OPN) expression of BMSCs cultured with different composite hydrogels. (*$p < 0.05$, ***$p < 0.001$)

containing 20% BG (0.27 U/L) (Fig. 6c). Regarding gene expression analyzed by qPCR, the inclusion of 5%, 10%, and 20% BG hydrogels significantly enhanced the expression of OPN when BMSCs were cultured for 7 days. Additionally, after 14 days, incorporating a 20% BG composite hydrogel increased the expression levels of ALP (9.1 times), RUNX2 (2.7 times), and OPN (2.3 times) in BMSCs (Fig. 6e-f). ALP is an early indicator of osteogenesis and closely correlates with the biomineralization process. RUNX2 and OPN are crucial ECM proteins that serve dual functions, playing a pivotal role in the survival of osteoclasts as well as bone mineralization [44]. The hydrogels containing 20% BG exhibited the highest capacity for mineralized crystal formation, which may transiently impede cell proliferation but ultimately promote osteogenic differentiation. Consequently, this particular group was chosen for in vivo experimentation. Therefore, adding bioglass releases various ions, such as calcium, phosphorus, and silicon ions, and these can produce phosphate crystals when in contact with body fluids. Such crystals have a high hardness, which can constitute both the bone mechanism and the signal for osteogenic differentiation that can be generated for stem cells, promoting the expression of osteogenesis-related genes such as ALP, RUNX2, OPN, which is conducive to the differentiation of cells to osteoblasts.

#### Bone regeneration promoted by composite hydrogels in vivo

To evaluate the osteogenic potential of the composite hydrogels in vivo, we initially implanted the lyophilized hydrogels into the subcutaneous tissue of rats. Subsequently, we obtained samples for Micro-CT analysis after 2 and 4 weeks. Compared to hydrogels without fibers, composite hydrogels containing fibers showed significantly enhanced mineralization after 2 and 4 weeks in vivo (Fig. S8). The fibers may offer additional attachment sites to form mineralized crystals, promoting crystal nucleation and subsequent crystal growth. Subsequently, a rat skull defect model was established, and the composite hydrogel was injected into the defect site, followed by UV light curing for 10 s. The samples were collected and analyzed by Micro-CT at 4, 8, and 12 weeks. Subsequently, the samples were decalcified, sectioned, and stained with H&E, Masson's trichrome stain, and immunohistochemical staining (Fig. 7a). The 20% BG composite hydrogel demonstrated significant osteogenesis in Micro-CT detection compared to the other groups at all three-time points (Fig. 7b). Moreover, although the presence of coaxial fibers did not exert a significant effect on bone regeneration, it was observed that the bone tended to be located more centrally within the skull defect. The quantitative bone volume/tissue volume (BV/TV) data was computed based on the 3D Micro-CT data. At 12 weeks, the 20% BG composite hydrogels repaired approximately 25% and 23% of the bone defects, which was much higher than the control group (10%) (Fig. 7c). This finding suggests that fibers may serve as nucleation sites for crystal formation, facilitating and enhancing bone regeneration. Currently, the prominence of 3D printing technology is driving advancements in bone formation, but it is challenging to apply to repair irregular defects [45, 46]. The strength of our study lies in its ability to cater to diverse application scenarios involving irregular defects while being easily implementable.

The results of H&E and Masson's trichrome staining of each group are presented in Fig. 8. The GelMA group was still not completely degraded at 4 weeks. However, upon the addition of BG, a substantial formation of blood tissue and bone-like matrix was observed, accompanied by an enhanced infiltration of lymphocytes. At 8 weeks, the BG group exhibited more multinucleated osteoclasts, while lymphocytes remained abundant. By 12 weeks, lymphocyte levels started to decline, accompanied by an increase in the quantity and size of the osteoid matrix and a significant reduction in the osteoclast population. As shown in Fig. 9a-b, hydrogels (including BG and coaxial fibers) dramatically increased the expression of OPN in immunohistochemical staining at all periods. Especially at 12 weeks, OPN expression in the GelMA-PCL@GelMA-BG group was 5 times higher than in the control group. CD31, a marker of nascent endothelial cells, is commonly employed for neonatal microvessel quantification to assess the angiogenesis of implanted materials [47, 48]. In immunohistochemical staining for CD31, the GelMA-PCL@GelMA-BG group had more CD31 expression and more vascular tissue production at 8 and 12 weeks (Fig. 9c-d). The observed results may be attributed to the synergistic interaction between the hydrogel matrix and the particles released from BG. In the GelMA-BG group, a substantial amount of CD31-labeled cavity formation was observed, which was infrequent in the GelMA-PCL@GelMA-BG group. Consequently, these findings suggest that including coaxial fibers effectively restricts cavity formation. It has been demonstrated that silicates can upregulate nitric oxide synthase, thereby inducing angiogenesis [49]. Calcium ions also facilitate angiogenesis, thereby augmenting the secretion of vascular-related cytokines and promoting endothelial cell adhesion [50]. BG, which releases calcium ions, may facilitate this process. Moreover, blood vessels can deliver nutrients, bioactive factors, and osteogenesis-related cells to promote new bone formation and

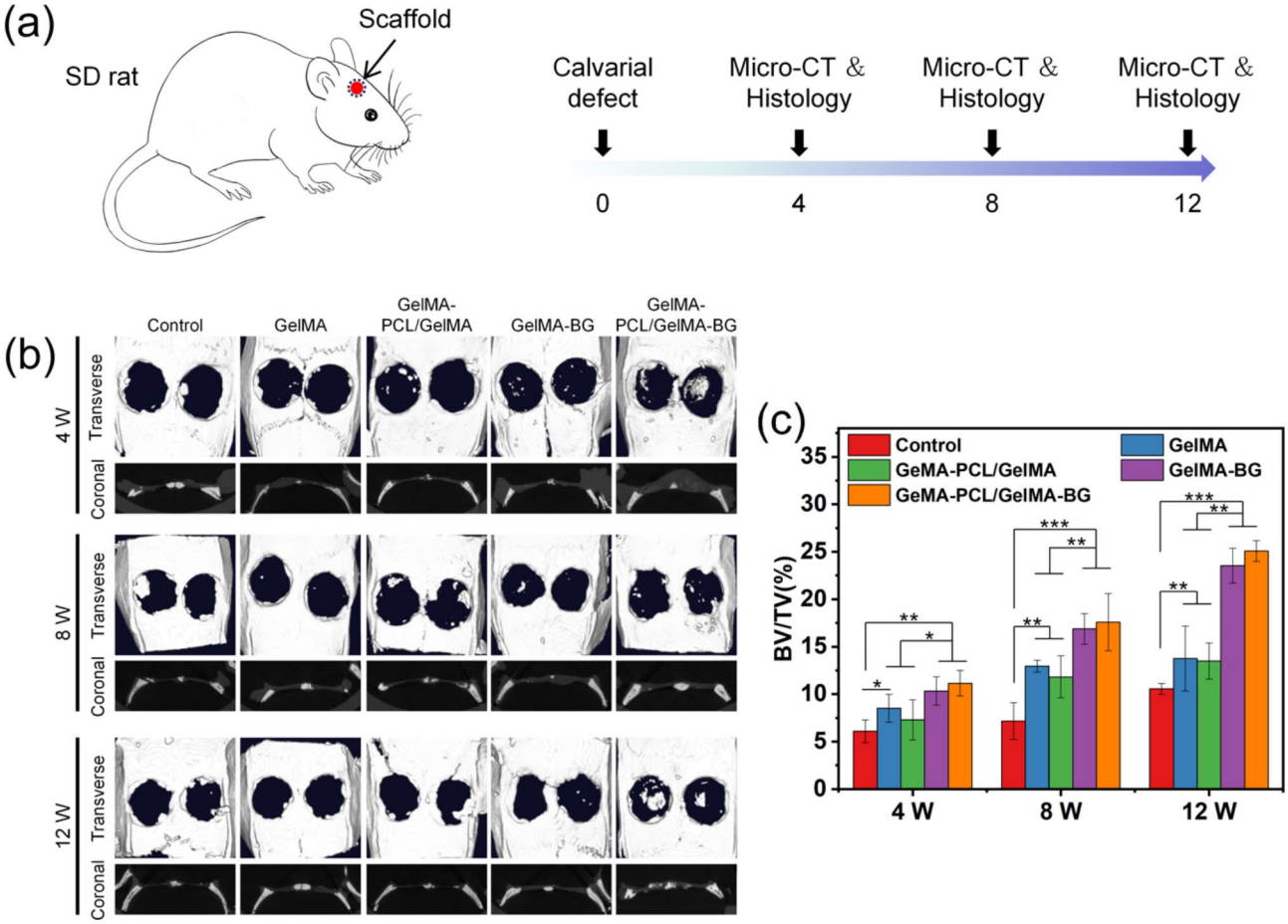


**Fig. 7** The animal experiment patterns and analysis of Micro-CT results. (**a**) The skull defect model of 6 mm diameter was established, and the samples were analyzed at 4, 8, and 12 weeks. (**b**-**c**) Micro-CT results showed that adding BG and coaxial fiber induced more bone regeneration. (*$p < 0.05$, **$p < 0.01$, ***$p < 0.001$)

transport metabolic waste or toxic products for accelerated repair. In conclusion, the novel advantages of the GelMA/BG-Fiber composite hydrogel enhanced biocompatibility and improved osteogenic and angiogenic marker expression, which are crucial for promoting bone regeneration.

Notwithstanding the preliminary findings of the present study, certain limitations were identified. For instance, the composite hydrogel displays inadequate strength, rendering it incapable of providing adequate support for the bone defect at the weight-bearing site. Consequently, it can only be employed as an auxiliary measure subsequent to internal fixation. Secondly, the hydrogel is of low viscosity, which carries the risk of detachment from the bone defect site. It is our intention to further improve the hydrogel composite in order to facilitate osteogenesis and vascularisation, which will be more pertinent to the context of bulk bone defect surgery.

## Conclusion

In summary, we have successfully demonstrated the development of a novel injectable osteogenic material by incorporating coaxial fibers, BG, and GelMA into a composite hydrogel. The BG component exhibits rapid ion release capabilities in physiological fluids, including Ca, P, and Si. Furthermore, it facilitates the formation of mineralized crystals on the surface and promotes hydroxyapatite deposition, which is essential for bone regeneration. The incorporation of PCL@GelMA coaxial nanofibers enhances the mechanical properties while preserving the pore structure of the composite hydrogels and provides additional nucleation sites for mineralized crystals, thereby facilitating the generation of a more significant number of mineralized crystals within the hydrogel. Such composite hydrogel induces enhanced expression of osteogenesis-related genes such as ALP, RUNX2, and OPN in vitro, while exhibiting augmented osteogenic and angiogenic capabilities in vivo, thereby holding potential for treating irregular bone defects.

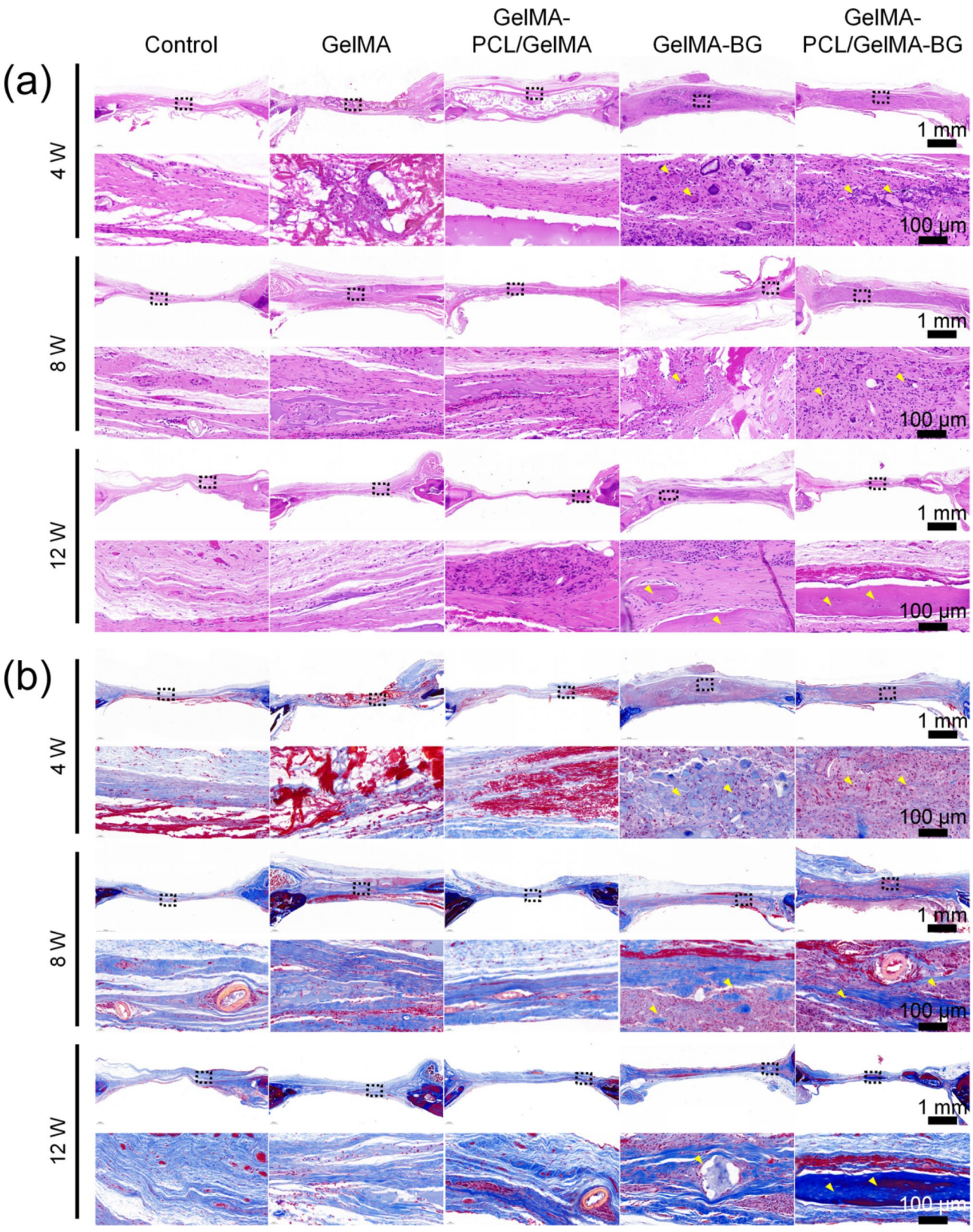


**Fig. 8** H&E and Masson's trichrome staining of the samples. (**a**-**b**) Adding BG and coaxial fibers promoted the early increase of osteoclasts and the formation of a bone-like matrix. The yellow arrows indicate the formation of a bone-like matrix and bone

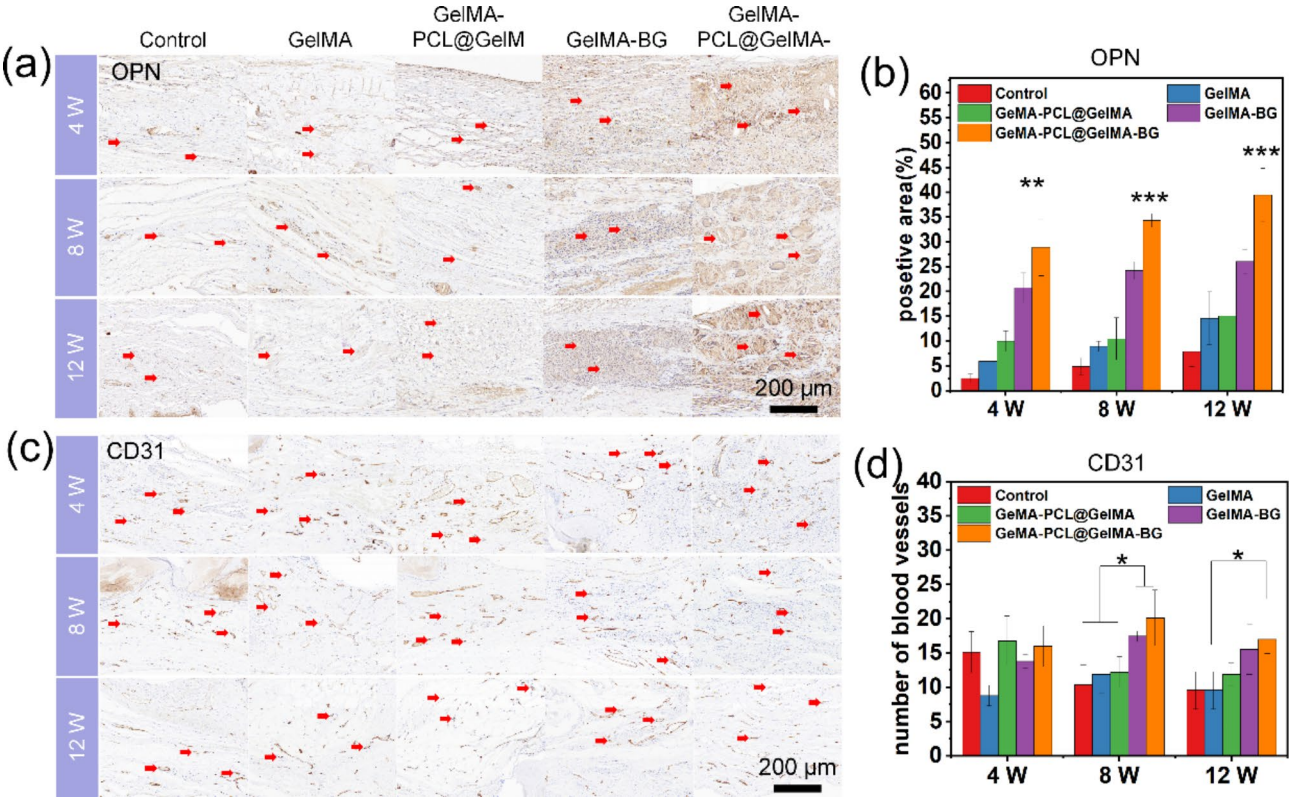


**Fig. 9** Immunohistochemical staining of the samples. (**a**-**b**) Immunohistochemical staining of osteoblastic marker (OPN) shows that the addition of BG and coaxial fibers promotes the expression of OPN. (**c**-**d**) Immunohistochemical staining of angiogenic marker (CD 31) shows that adding BG and coaxial fibers promotes the expression of CD 31 at 8 and 12 weeks. (*$p < 0.05$, **$p < 0.01$, ***$p < 0.001$)

## Supplementary Information

The online version contains supplementary material available at https://doi.org/10.1186/s12951-024-02980-w.

Supplementary Material 1

**Acknowledgements**
The authors thank the "Advanced Biomaterials and Regenerative Medicine" Innovation Team supported by the Young-Talent Introduction and Cultivation Plan in the Universities of Shandong Province.

**Author contributions**
Chenghao Yu: Conceptualization, Data curation, Formal analysis, Methodology, Validation, Visualization, Writing - original draft. Jinli Chen: Investigation, Data curation. Tianrui Wang: Formal analysis, Investigation, Methodology. Yawen Wang: Investigation, Methodology. Xiaopei Zhang: Investigation, Validation. Zhouli Zhang: Writing - review & editing. Yuanfei Wang: Investigation, Funding acquisition, Project administration, Supervision, Writing - review & editing. Tengbo Yu: Funding acquisition, Investigation, Project administration, Supervision, Writing - review & editing. Tong Wu: Conceptualization, Project administration, Funding acquisition, Investigation, Methodology, Supervision, Writing - review & editing.

**Funding**
This research was supported by the Natural Science Foundation of Shandong Province (ZR2021YQ17), the Special Funds for Taishan Scholars Project of Shandong Province (No. tsqn202211125), National Natural Science Foundation of China (32171322), Key Research and Development Program of Shandong Province (2021SFGC0502), Young Elite Scientists Sponsorship Program by CAST (No. YESS20200097), Natural Science Foundation of Shandong Province (ZR2021QC063), Qingdao Key Health Discipline Development Fund (2022–2024), Qingdao Clinical Research Center for Oral Diseases (22-3-7-lczx-7-nsh), and Shandong Provincial Key Medical and Health Discipline of Oral Medicine (2024–2026).

**Data availability**
The datasets used and/or analyzed during the current study are available from the corresponding author upon reasonable request.

## Declarations

**Ethics approval and consent to participate**
All animal experiment studies were approved by the animal ethics committee of Qingdao University (No.20210901SD5020231101128, Shandong, China) and conducted in accordance with the National Research Council's Guide for the Care and Use of Laboratory Animals.

**Consent for publication**
Not applicable.

**Competing interests**
The authors declare no competing interests.

Received: 7 July 2024 / Accepted: 4 November 2024
Published online: 11 November 2024

**References**

1. Yao Q, Li W, Yu S, Ma L, Jin D, Boccaccini AR, Liu Y. Multifunctional chitosan/polyvinyl pyrrolidone/45S5 Bioglass® scaffolds for MC3T3-E1 cell stimulation and drug release. Mater Sci Eng C Mater Biol Appl. 2015;56:473–80.
2. Keshavarz M, Alizadeh P, Kadumudi FB, Orive G, Gaharwar AK, Castilho M, Golafshan N, Dolatshahi-Pirouz A. Multi-leveled Nanosilicate implants

can facilitate Near-Perfect Bone Healing. ACS Appl Mater Interfaces. 2023;15:21476–95.
3. García-Gareta E, Coathup MJ, Blunn GW. Osteoinduction of bone grafting materials for bone repair and regeneration. Bone. 2015;81:112–21.
4. Wang Y, Wang J, Gao R, Liu X, Feng Z, Zhang C, Huang P, Dong A, Kong D, Wang W. Biomimetic glycopeptide hydrogel coated PCL/nHA scaffold for enhanced cranial bone regeneration via macrophage M2 polarization-induced osteo-immunomodulation. Biomaterials. 2022;285:121538.
5. Wu Z, Bai J, Ge G, Wang T, Feng S, Ma Q, Liang X, Li W, Zhang W, Xu Y, Guo K, Cui W, Zha G, Geng D. Regulating macrophage polarization in high glucose microenvironment using Lithium-modified Bioglass-Hydrogel for Diabetic Bone Regeneration. Adv Healthc Mater. 2022;11:e2200298.
6. Barreto MEV, Medeiros RP, Shearer A, Fook MVL, Montazerian M, Mauro JC. Gelatin and Bioactive Glass Composites for Tissue Engineering: a review. J Funct Biomater. 2022;14:23.
7. Zheng X, Zhang X, Wang Y, Liu Y, Pan Y, Li Y, Ji M, Zhao X, Huang S, Yao Q. Hypoxia-mimicking 3D bioglass-nanoclay scaffolds promote endogenous bone regeneration. Bioact Mater. 2021;6:3485–95.
8. Hentrich RL, Graves GA, Stein HG, Bajpai PK. An evaluation of inert and resorbable ceramics for future clinical orthopedic applications. J Biomed Mater Res. 1971;5:25–51.
9. Zheng J, Zhao F, Zhang W, Mo Y, Zeng L, Li X, Chen X. Sequentially-crosslinked biomimetic bioactive glass/gelatin methacryloyl composites hydrogels for bone regeneration. Mater Sci Eng C Mater Biol Appl. 2018;89:119–27.
10. Wilson J, Low SB. Bioactive ceramics for periodontal treatment: comparative studies in the Patus monkey. J Appl Biomater. 1992;3:123–9.
11. Borden M, Westerlund LE, Lovric V, Walsh W. Controlling the bone regeneration properties of bioactive glass: effect of particle shape and size. J Biomed Mater Res B Appl Biomater. 2022;110:910–22.
12. Jell G, Notingher I, Tsigkou O, Notingher P, Polak JM, Hench LL, Stevens MM. Bioactive glass-induced osteoblast differentiation: a noninvasive spectroscopic study. J Biomed Mater Res A. 2008;86:31–40.
13. Gorustovich AA, Roether JA, Boccaccini AR. Effect of bioactive glasses on angiogenesis: a review of in vitro and in vivo evidences. Tissue Eng Part B Rev. 2010;16:199–207.
14. Naruphontjirakul P, Kanchanadumkerng P, Ruenraroengsak P. Multifunctional zn and ag co-doped bioactive glass nanoparticles for bone therapeutic and regeneration. Sci Rep. 2023;13:6775.
15. Kargozar S, Montazerian M, Fiume E, Baino F. Multiple and promising applications of Strontium (Sr)-Containing bioactive glasses in bone tissue Engineering. Front Bioeng Biotechnol. 2019;7:161.
16. Kurtuldu F, Mutlu N, Michálek M, Zheng K, Masar M, Liverani L, Chen S, Galusek D, Boccaccini AR. Cerium and gallium containing mesoporous bioactive glass nanoparticles for bone regeneration: Bioactivity, biocompatibility and antibacterial activity. Mater Sci Eng C Mater Biol Appl. 2021;124:112050.
17. Liu M, Zeng X, Ma C, Yi H, Ali Z, Mou X, Li S, Deng Y, He N. Injectable hydrogels for cartilage and bone tissue engineering. Bone Res. 2017;5:17014.
18. Bello AB, Kim D, Kim D, Park H, Lee SH. Engineering and functionalization of gelatin biomaterials: from Cell Culture to Medical Applications. Tissue Eng Part B Rev. 2020;26:164–80.
19. Dimatteo R, Darling NJ, Segura T. In situ forming injectable hydrogels for drug delivery and wound repair. Adv Drug Deliv Rev. 2018;127:167–84.
20. Qiu W, Han H, Li M, Li N, Wang Q, Qin X, Wang X, Yu J, Zhou Y, Li Y, Li F, Wu D. Nanofibers reinforced injectable hydrogel with self-healing, antibacterial, and hemostatic properties for chronic wound healing. J Colloid Interface Sci. 2021;596:312–23.
21. Arambula-Maldonado R, Liu Y, Xing M, Mequanint K. Bioactive and electrically conductive GelMA-BG-MWCNT nanocomposite hydrogel bone biomaterials. Biomater Adv. 2023;154:213616.
22. Loessner D, Meinert C, Kaemmerer E, Martine LC, Yue K, Levett PA, Klein TJ, Melchels FP, Khademhosseini A, Hutmacher DW. Functionalization, preparation and use of cell-laden gelatin methacryloyl-based hydrogels as modular tissue culture platforms. Nat Protoc. 2016;11:727–46.
23. Zhu M, Wang Y, Ferracci G, Zheng J, Cho NJ, Lee BH. Gelatin methacryloyl and its hydrogels with an exceptional degree of controllability and batch-to-batch consistency. Sci Rep. 2019;9:6863.
24. Shirahama H, Lee BH, Tan LP, Cho NJ. Precise tuning of Facile One-Pot gelatin methacryloyl (GelMA) synthesis. Sci Rep. 2016;6:31036.
25. Ganguly K, Dutta SD, Randhawa A, Patel DK, Patil TV, Lim KT. Transcriptomic changes toward osteogenic differentiation of mesenchymal stem cells on 3D-Printed GelMA/CNC Hydrogel under pulsatile pressure environment. Adv Healthc Mater. 2023;12:2202163.
26. Barabadi Z, Azami M, Sharifi E, Karimi R, Lotfibakhshaiesh N, Roozafzoon R, Joghataei MT, Ai J. Fabrication of hydrogel based nanocomposite scaffold containing bioactive glass nanoparticles for myocardial tissue engineering. Mater Sci Eng C Mater Biol Appl. 2016;69:1137–46.
27. Levengood SL, Zhang M. Chitosan-based scaffolds for bone tissue engineering. J Mater Chem B. 2014;2:3161–84.
28. Houaoui A, Szczodra A, Lallukka M, El-Guermah L, Agniel R, Pauthe E, Massera J, Boissiere M. New generation of hybrid materials based on gelatin and bioactive glass particles for bone tissue regeneration. Biomolecules. 2021;11:444.
29. Deguchi K, Nomura S, Tsuchiya A, Takahashi I, Ishikawa K. Effects of the carbonate content in carbonate apatite on bone replacement. J Tissue Eng Regen Med. 2022;16:200–6.
30. Guo W, Zhao F, Wang Y, Tang J, Chen X. Characterization of the mechanical behaviors and bioactivity of tetrapod ZnO whiskers reinforced bioactive glass/gelatin composite scaffolds. J Mech Behav Biomed Mater. 2017;68:8–15.
31. Liu YN, Guo QX, Zhang XP, Wang YF, Mo XM, Wu T. Progress in Electrospun fibers for manipulating cell behaviors. Adv Fiber Mater. 2023;5(4):1241–72.
32. Deng X, Yu C, Zhang X, Tang X, Guo Q, Fu M, Wang Y, Fang K, Wu T. A chitosan-coated PCL/nano-hydroxyapatite aerogel integrated with a nanofiber membrane for providing antibacterial activity and guiding bone regeneration. Nanoscale. 2024;16:9861–74.
33. Yu CH, Wang TR, Diao HC, Liu N, Zhang Y, Jiang HY, Zhao P, Shan ZY, Sun ZW, Wu T, et al. Photothermal-triggered structural change of Nanofiber Scaffold integrating with graded mineralization to promote Tendon-Bone Healing. Adv Fiber Mater. 2022;4(4):908–22.
34. Yu C, Chen R, Chen J, Wang T, Wang Y, Zhang X, Wang Y, Wu T, Yu T. Enhancing tendon-bone integration and healing with advanced multi-layer nanofiber-reinforced 3D scaffolds for acellular tendon complexes. Mater Today Bio. 2024;26:101099.
35. Oonishi H, Hench LL, Wilson J, Sugihara F, Tsuji E, Matsuura M, Kin S, Yamamoto T, Mizokawa S. Quantitative comparison of bone growth behavior in granules of Bioglass, A-W glass-ceramic, and hydroxyapatite. J Biomed Mater Res. 2000;51:37–46.
36. Hattori K, Hayakawa S, Shirosaki Y. Effects of the silicon-containing chemical species dissolved from chitosan-siloxane hybrids on nerve cells. J Solgel Sci Technol. 2022;104:606–16.
37. Oudadesse H, Najem S, Mosbahi S, Rocton N, Refifi J, El Feki H, Lefeuvre B. Development of hybrid scaffold: bioactive glass nanoparticles/chitosan for tissue engineering applications. J Biomedical Mater Res Part A. 2021;109:590–9.
38. Bellucci D, Salvatori R, Giannatiempo J, Anesi A, Bortolini S, Cannillo V. A New Bioactive Glass/Collagen Hybrid Composite for Applications in Dentistry. Mater (Basel). 2019;12:2079.
39. Gong W, Liu L, Luo L, Ji L. Preparation and characterization of a self-cross-linking sodium alginate-bioactive glass sponge. J Biomed Mater Res B Appl Biomater. 2023;111:173–83.
40. Lin Z, Tao Y, Huang Y, Xu T, Niu W. Applications of marine collagens in bone tissue engineering. Biomed Mater. 2021;16:042007.
41. Kirsch M, Birnstein L, Pepelanova I, Handke W, Rach J, Seltsam A, Scheper T, Lavrentieva A. Gelatin-methacryloyl (GelMA) formulated with human platelet lysate supports mesenchymal stem cell proliferation and differentiation and enhances the Hydrogel's Mechanical properties. Bioeng (Basel). 2019;6:76.
42. Siqueira RL, Maurmann N, Burguês D, Pereira DP, Rastelli ANS, Peitl O, Pranke P, Zanotto ED. Bioactive gel-glasses with distinctly different compositions: Bioactivity, viability of stem cells and antibiofilm effect against Streptococcus mutans. Mater Sci Eng C Mater Biol Appl. 2017;76:233–41.
43. Thakur T, Xavier JR, Cross L, Jaiswal MK, Mondragon E, Kaunas R, Gaharwar AK. Photocrosslinkable and elastomeric hydrogels for bone regeneration. J Biomed Mater Res A. 2016;104:879–88.
44. Marycz K, Śmieszek A, Kornicka-Garbowska K, Pielok A, Janeczek M, Lipińska A, Nikodem A, Filipiak J, Sobierajska P, Nedelec JM, Wiglusz RJ. Novel nano-hydroxyapatite (nHAp)-Based Scaffold Doped with Iron Oxide nanoparticles (IO), functionalized with small non-coding RNA (miR-21/124) modulates expression of runt-related transcriptional factor 2 and Osteopontin, promoting regeneration of osteoporotic bone in bilateral cranial defects in a senescence-accelerated mouse model (SAM/P6). PART 2. Int J Nanomed. 2021;16:6049–65.
45. Yang C, Ma H, Wang Z, Younis MR, Liu C, Wu C, Luo Y, Huang P. 3D printed Wesselsite Nanosheets Functionalized Scaffold facilitates NIR-II Photothermal Therapy and Vascularized Bone Regeneration. Adv Sci (Weinh). 2021;8:e2100894.

46. Tulyaganov DU, Fiume E, Akbarov A, Ziyadullaeva N, Murtazaev S, Rahdar A, Massera J, Verné E, Baino F. Vivo evaluation of 3D-Printed silica-based Bioactive Glass scaffolds for Bone Regeneration. J Funct Biomater. 2022;13:74.
47. Xin T, Gu Y, Cheng R, Tang J, Sun Z, Cui W, Chen L. Inorganic strengthened Hydrogel membrane as regenerative Periosteum. ACS Appl Mater Interfaces. 2017;9:41168–80.
48. Hao ZW, Chen TH, Wang Y, Feng QY, Chen JY, Li HK, Wang JW, Wang ZP, Zhang ZY, Chen RX, et al. Self-assembling peptide nanofibers anchored parathyroid hormone derivative for bone tissue Engineering. Adv Fiber Mater. 2024;6:583–606.
49. Liu X, Zhao N, Liang H, Tan B, Huang F, Hu H, Chen Y, Wang G, Ling Z, Liu C, Miao Y, Wang Y, Zou X. Bone tissue engineering scaffolds with HUVECs/hBMSCs cocultured on 3D-printed composite bioactive ceramic scaffolds promoted osteogenesis/angiogenesis. J Orthop Translat. 2022;37:152–62.
50. Aguirre A, González A, Planell JA, Engel E. Extracellular calcium modulates in vitro bone marrow-derived Flk-1 + CD34 + progenitor cell chemotaxis and differentiation through a calcium-sensing receptor. Biochem Biophys Res Commun. 2010;393:156–61.

## Publisher's note

Springer Nature remains neutral with regard to jurisdictional claims in published maps and institutional affiliations.